Earthquake Research Advances 6 (2026) 100376

Contents lists available at ScienceDirect

Earthquake Research Advances

journal homepage: www.keaipublishing.com/en/journals/earthquake-research-advances

Using historical remote sensing images for detailed tectonic geomorphological interpretation in the study of active faults: Application to the Xiaojiang fault case study

Xingao Li [a], Zhongtai He [b,c,*], Long Guo [b,c], Linlin Li [a]

[a] National Institute of Natural Hazards, Ministry of Emergency Management of China, Beijing, 100085, China
[b] State Key Laboratory of Earthquake Dynamics and Forecasting, Institute of Geology, China Earthquake Administration, Beijing, 100029, China
[c] Key Laboratory of Seismic and Volcanic Hazards, Institute of Geology, China Earthquake Administration, Beijing, 100029, China

ARTICLE INFO

Keywords:
Historical remote sensing image
Remote sensing interpretation
Xiaojiang fault
Active fault

ABSTRACT

The northern section of the Xiaojiang fault is the most active section in the Xiaojiang Fault Zone, and a detailed interpretation of this fault is highly important. In this work, KeyHole-4B images and Landsat 8 images of the northern section of the Xiaojiang fault were collected, and remote sensing interpretation and tectonic geomorphological analysis of the northern section of the Xiaojiang fault were carried out to obtain a more detailed fault distribution. The results reveal that the northern section of the Xiaojiang fault is a group of faults that are subparallel to each other with a space of 2–4 km. The fault is located along the Jinshajiang Valley and the Xiaojiang Valley. At the same time, we counted the large-scale left-lateral dislocations of the gullies and ridges. Combined with the results of previous studies, the long-term average slip rate of the northern section of the Xiaojiang fault is 6.2 ± 1.1 mm/a since the late Middle Pleistocene, 11.4 ± 2.8 mm/a since the middle of the late Pleistocene, and 8.0 ± 2.0 mm/a since the middle and late Pleistocene. The high slip rate in the northern section of the Xiaojiang fault represents the response of the local strain of the central Yunnan subblock, which rotates clockwise along the boundary fault. This finding is consistent with the pattern of northwards and north-east wards thrusting of the Indian plate, leading to eastwards extrusion and the escape of material from the Qinghai-Xizang Plateau.

1. Introduction

In the 1970s, Molnar and Tapponnier pioneered the use of Landsat Multispectral Scanner (MSS) satellite imagery to study the major active rupture features in the vicinity of East Asian (Molnar and Tapponnier, 1975), especially on the Qinghai-Xizang Plateau (Qingzang Plateau), and proposed the famous 'continental escape' hypothesis. Multisource remote sensing data can objectively reflect the geometry and distribution of active faults at the macro scale, and the emergence of high-resolution remote sensing products provides a convenient and reliable means for studying active faults in detail. Remote sensing research on active faults has fundamentally improved upon conventional methods of investigating active faults that are limited by factors such as the topography of the study area, the climate and the subjective awareness of individuals. Remote sensing images have gradually become important basic data for active fault research, and interpreting remote sensing images has also become a fundamental task in this field. This research can reveal the features of active faults at different spatiotemporal scales to other researchers (Zhang et al., 2016).

Holocene faults formed typical tectonic landforms in the process of surface shaping and generated geomorphological dislocation units with significance. Morphological analysis of Late Quaternary tectonic landforms within the influence of the fault zone can effectively reveal the kinematic characteristics of the faults and their evolutionary patterns (Zielke et al., 2012). Typical active faults often develop tectonic geomorphological assemblages, such as stepped fault scarp, linear valley, and tensile fault basin, accompanied by secondary geomorphological responses, including water system offset, terrace sequence dislocation, and alluvial fan deformation. Topography and geomorphology can not only indicate the location of active fault development, but also accurately

* Corresponding author. State Key Laboratory of Earthquake Dynamics and Forecasting, Institute of Geology, China Earthquake Administration, Beijing, 100029, China.
E-mail addresses: lixingao2021@126.com (X. Li), hzt@ies.ac.cn (Z. He), guolong1115@163.com (L. Guo), leein@sina.com (L. Li).
Peer review under the responsibility of Editorial Board of Earthquake Research Advances.

https://doi.org/10.1016/j.eqrea.2025.100376
Received 17 February 2025; Received in revised form 31 March 2025; Accepted 31 March 2025
2772-4670/© 2025 The Authors. Publishing services by Elsevier B.V. on behalf of KeAi Communications Co. Ltd. This is an open access article under the CC BY-NC-ND license (http://creativecommons.org/licenses/by-nc-nd/4.0/).

record the direction and scale of fault seismic displacement (Jiang et al., 2017; Jiang, 2018).

The slip rate of a strike-slip fault is the average slip of fault movement in a certain period of time, which reflects the rate of energy accumulation on a strike-slip fault zone, and can be applied to the probability evaluation of seismic risk (Molnar and Tapponnier, 1978; Zhang et al., 2008). The fault movement is based on the elastic rebound theory conceptually (Reid, 1910), where elastic strain energy accumulates across a locked fault until a critical threshold is reached, at which time the stored energy is 'instantaneously' released as seismic waves (Gold et al., 2017; Scholz, 2019). During this process, the surface drainages, ridges, river terraces, or their intervening risers, alluvial fans, moraines, shorelines, and other landforms crossing the fault will be displaced along the relative movement direction of the two walls of the fault. These offset geomorphic markers can be preserved for thousands of years or even longer under appropriate external conditions, to record the displacement and movement sense on the surface during the earthquake. Considering that linear landforms can be easily restored to their original shape and position, the identification of these linear geomorphic markers is an effective means to quantify the amount of seismic deformation (Dong, 2015). At present, it is generally used to calculate the slip rate of active strike-slip faults based on the accumulated displacements of the offset landforms and the corresponding ages (Sieh and Jahns, 1984; Weldon and Sieh, 1985; Zhang et al., 2008). Because the corresponding cumulative time is difficult to measure directly, it is often constrained by the age of the geomorphic surface (Liu et al., 2021).

The Xiaojiang Fault Zone is large with left-lateral and slip, one of the boundary faults between the rhombic Sichuan-Yunnan Block and South China Block, and an important part of the north-south seismic zone (Cheng et al., 2021; Guo et al., 2021). Due to the interaction between the Indian and Eurasian plates, the Xiaojiang Fault Zone has become one of the most seismically active deep and large faults in China and has experienced numerous destructive earthquakes in its history (Guo et al., 2021). Due to its strong activity, scholars have studied the tectonics, topographic and geomorphological features, and neotectonic activity of this fault zone (Han et al., 2017; Chang et al., 2021; Guo et al., 2021; Hu et al., 2023). In recent studies, geophysical methods or high-resolution remote sensing images have often been used to study the spreading and deep tectonics of faults (Yi et al., 2008; Mao et al., 2016; Li et al., 2020; Meng et al., 2021). Owing to the accelerated pace of urbanization, the topography and geomorphology of many areas have been damaged, and determining the detailed geometry of the spreading of the entire fault section via high-resolution remote sensing images is impossible. Previous generations have argued that the northern section of the Xiaojiang fault (XJF) has been characterized by a simple structure and distinct geomorphological phenomena (Mao et al., 2016; Li et al., 2020). Previous interpretations of the geomorphological features of the XJF utilized multisource remote sensing images to propose its geometrical spreading characteristics (Li et al., 2020). However, the interpretation of the northern section primarily reveals the development of linear gully landforms along the Jinshajiang and Xiaojiang Valleys, lacking a more detailed analysis (Li et al., 2020). Anthropogenic factors, necessitating consideration of human influences in the assessment of linear geomorphology, have significantly impacted this area. Consequently, the interpretation of active faults through remote sensing data often overlooks the tectonic and geomorphological features at smaller scales, which can hinder the accurate localization of the geometrical spread of these faults. The XJF has undergone substantial modification due to various tectonic movements over a long evolutionary period and extensive spatial range, resulting in a complex tectonic pattern. Historically, investigations have concentrated on the central and southern parts of the XJF, while the northern section has received comparatively less attention.

The landforms in early historical aerial photographs and images taken in the 1960s and 1970s were not artificially altered, preserving the original geomorphic information and facilitating fault interpretation. The northern section of the XJF is located in a subtropical climate with dense vegetation cover and is partly located in the mountains, which makes transportation difficult and makes it difficult to carry out field investigations in many sections. These difficulties can be mitigated only by detailed remote sensing interpretation. In this study, Landsat 8 and KeyHole-4B (KH-4B) images of the northern section of the XJF are collected, and a detailed interpretation is conducted to ascertain the precise geometric spread of this section. Concurrently, the long-term slip rate of the northern section of the XJF is estimated, and the motion model of the Sichuan-Yunnan block on the southeastern margin of the Qingzang Plateau is explored.

2. Regional tectonic background

The subduction and collision of the Indian Plate with the Eurasian Plate in the early Cenozoic led to the rapid uplift of the Qingzang Plateau and strong deformation around the plateau (Fig. 1b) (Molnar and Tapponnier, 1975). The Sichuan–Yunnan Block is located on the southeastern margin of the Qingzang Plateau and is bordered by the South China Block in the east. Due to the convergence and extrusion of the Indian and Eurasian Plates, the massif moves in a south-southeast direction (Wang and Burchfiel, 2000; Schoenbohm et al., 2006; Zheng et al., 2017). The southeastern part of the Sichuan-Yunnan block features two groups of near N-S- and NW-WNW-oriented active faults with different directions (Fig. 1a). The Xiaojiang Fault Zone is internally intersected by faults, with a nearly N-S strike and a total length of approximately 400 km, and is characterized by strike-slip movement with left-lateral, with an overall eastwards slightly convex arc spreading zone (Song et al., 1998; Han et al., 2017). The Sichuan-Yunnan block moves southeastward at 3–5 mm/a (Burchfiel et al., 2003), whereas the southeastward extruding component of the South China Block moves at approximately 20 mm/a (Zhang et al., 2004).

The formation of the Xiaojiang fault originated with the Jinning movement at the end of the Middle Proterozoic (Song et al., 1998; Wang and Burchfiel, 2000). Following a prolonged period of geological evolution, particularly since the Cenozoic, the Xishan movement has played a significant role in uplifting the Qinghai-Xizang Plateau, thereby exerting pressure on the Sichuan-Yunnan rhombic fault block, which is driven eastward. Under regional tectonic stress, the diamond-shaped block continues to move in a south-southeast direction, resulting in a transition of the eastern boundary of the block—Xiaojiang fault activity—from extrusion to a left-rotating slip and thrust. The northern section of the XJF extends along the Jinsha River and Xiaojiang valleys, functioning as an active fault zone primarily characterized by left-lateral strike-slip motion (Song et al., 1998). Geomorphologically, it manifests as a large-scale fault trough formed by river erosion along the fault zone. In the middle and northern sections of the XJF, significant activity during the Pleistocene is evident, with observable surface rupture zones, stratigraphic faults from the fourth series, twisted water system ridges, hot springs, and high-temperature carbonation anomalies, all of which are indicative of fault activity. Since the Cenozoic era, fault activity has gradually shifted toward slip. The fault traverses various water systems and mountain ridges, where geological displacement phenomena are pronounced. Along the fault zone, geomorphological features such as fault troughs, steep cliffs, and faulted basins are clearly developed in the longitudinal direction of the faults.

The Xiaojiang Fault Zone is also the fault zone with the largest number of $M \geq 7$ earthquakes in Yunnan, and it is the most significant earthquake-controlled tectonic zone in Yunnan. According to historical seismic records, 17 $M \geq 6$ earthquakes occurred along the Xiaojiang Fault zone, including 4 $M \geq 7$ earthquakes and 1 M 8 earthquake, and all $M \geq 7$ earthquakes were located in the Xiaojiang Fault Zone, with the largest magnitude earthquake being the 1833 Songming M 8 earthquake (Song et al., 1998). The four $M \geq 7$ earthquakes were all concentrated in the northern and central parts of the Xiaojiang Fault Zone, namely, the 1500 Yiliang M 7 earthquake, the 1733 Dongchuan M 7¾ earthquake, the 1789

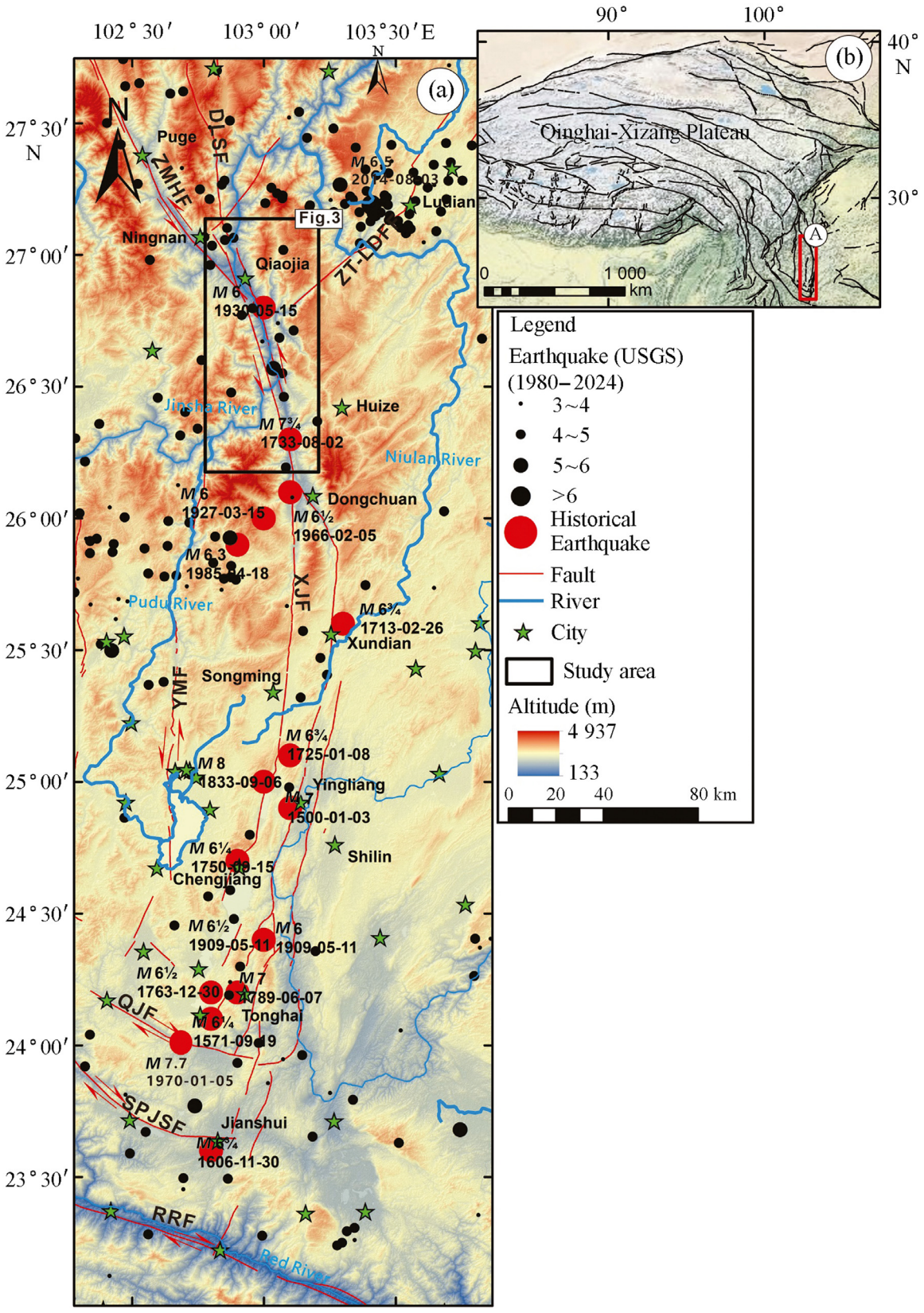

Fig. 1. Maps of the regional topography, active tectonics, and historical earthquakes. (a) Distribution of the Xiaojiang fault; (b) distribution of the Qingzang Plateau and peripheral faults.
ZMHF: Zemuhe fault; XJF: Xiaojiang fault; YMF: Yuanmou fault; QJF: Qujiang fault; SPJSF: Shiping-Jianshui fault; RRF: Red River fault; ZT-LDF: Zhaotong-Ludian fault.

Huaning *M* 7 earthquake, and the 1833 Chongming *M* 8 earthquake (Tan et al., 2023). In 1733, the *M* 7¾ Dongchuan 1733 earthquake occurred in the northern section of the Xiaojiang fault (XJF).

In terms of regional tectonics, the northern section of the XJF is at the intersection of the Zemuhe fault, the Daliangshan fault, and the Zhaotong-Ludian fault, and the northern section and the Zemuhe fault have formed a 4.5-km-wide pull-out tectonics in the Ningnan Basin (Wang et al., 2024a, 2024b), which constitutes a geometrical obstacle to seismic rupture. The northern section is intersected by the Daliangshan fault near Qiaojia in a 'Y' shape, which lacks significant structural barriers and has the risk of cascading rupture (Wang et al., 2024a, 2024b). Historical seismic activity shows that the 1733 Dongchuan *M* 7¾ earthquake and the 2014 Ludian *M* 6.5 earthquake are associated with tectonic activity in this section (Li et al., 2015).

3. Data and methods

3.1. Data selection

The remote sensing data used in this paper include Landsat 8 and KH-4B satellite images. The Google Earth and Landsat 8 images were used as the baseline, and the intersection points of the water system, which are not easy to change, were used as the characteristic points to align the two historical images on the basis of the relative relationship of the unchanged features (Wang et al., 2018). This step was taken so that the images that aligned with the historical remote sensing data could be used to measure the size of dislocation of the gully ridges, etc. (Fig. 2a and b), and to carry out research on faults. Because the KH-4B image is a two-dimensional image, it is suitable for a strike-slip fault. The selected Landsat 8 constitutes a medium-resolution optical image, suitable for macroscopic judgements about the spatial distribution of fault structures. Due to the large-scale engineering construction that has taken place in most parts of the northern section of the research area, the original landform has been destroyed. As a result, KH-4B satellite images have been selected.

Landsat 8 satellite data were selected, and the selected image was taken on January 18, 2020. The Landsat 8 satellite carries an operational land imager (OLI) and a thermal infrared sensor (TIRS) with 11 bands, and the spatial resolution of bands 2–7 (multispectral band) is 30 m. Bands 10 and 11 are thermal infrared bands with a spatial resolution of 100 m, and band 8 is a panchromatic band. The spatial resolution of the 2^{nd}—7^{th} bands (multispectral bands) is 30 m; the 10th and 11th bands are thermal infrared bands with a spatial resolution of 100 m; and the 8th band is a panchromatic band with a spatial resolution of 15 m (Zhao, 2003; Zhao et al., 2019). The selected KH-4B image was taken in 1968 (https://earthexplorer.usgs.gov/) and has a resolution of approximately 1.8 m. The main technical parameters of the satellite are as follows: (1) film-type camera, with a 70 mm negative; (2) panchromatic band imaging (black and white); (3) focal length of 61 mm; (4) nominal orbital altitude of 150 m; and (5) optimal ground resolution of 1.8 m. These types of images were located by manually adding ground control points. The optimal ground resolution was 1.8 m. Both image types were positioned manually by adding ground control points. Remote sensing interpretation was performed via historical aerial photographs and KH-4B satellite imagery, which has also been widely used in studies on the Yishu Fault Zone (Jiang et al., 2017).

Modern high-resolution datasets, such as LiDAR measurement technology, with its advantages of high precision, omni-directional, direct and rapid acquisition of three-dimensional spatial information on the target surface, can provide active tectonic research with high-precision geomorphological elevation base data along the entire fault zone (Bi et al., 2022), and deep seismic reflection profiles can obtain images of the crust's fine structure and the deep and shallow tectonic features of the faults (Yan et al., 2020). In general, LiDAR data are more reliable for areas with less human damage, and can penetrate vegetation, measure minor dislocations (including horizontal and vertical dislocations), and better reflect the fine tectonic deformation characteristics of typical dislocation points. However, the lidar data, deep seismic reflection profiles need to be actively acquired and the cost is high, and most of the northern section of the XJF is in the valley area, which has been massively damaged by human beings, which is not conducive to the interpretation of the lidar data. KH-4B satellite data have the advantages

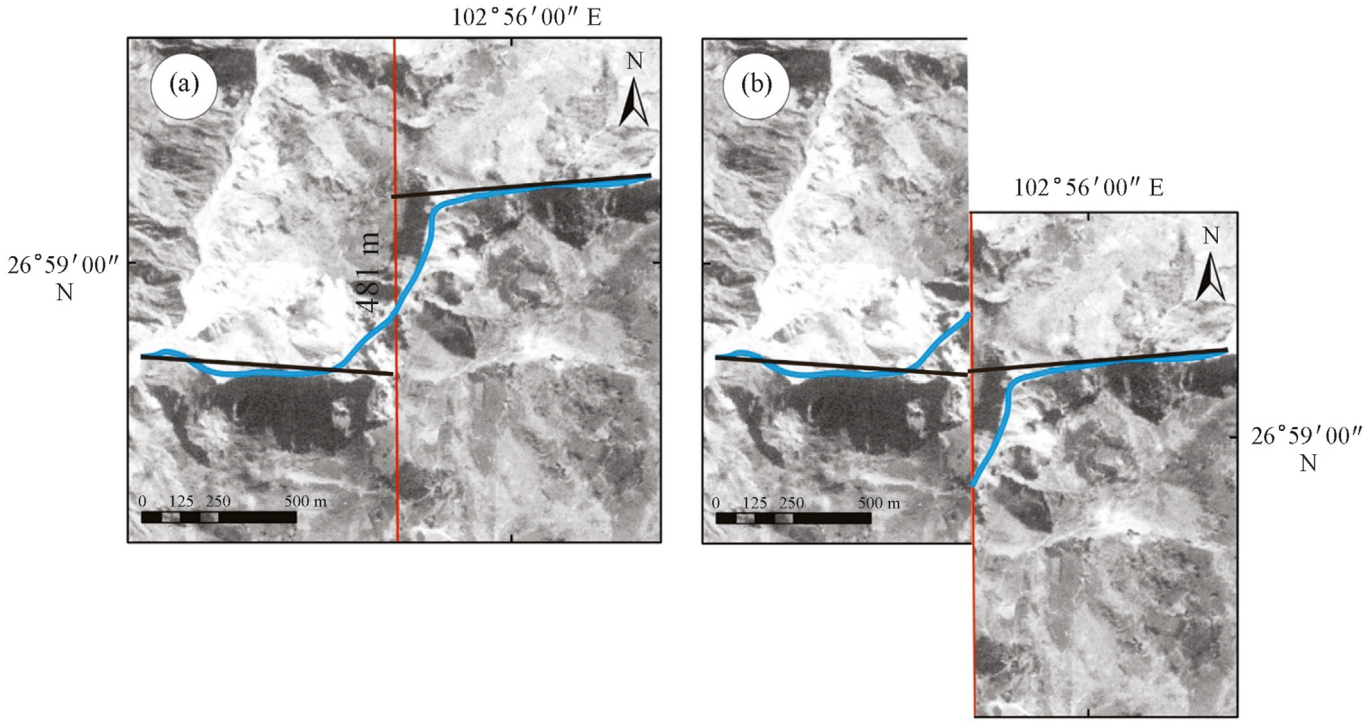

Fig. 2. Example of measured dislocations in historical images. The blue line represents the river, the red line represents the fault, and the black line represents the alignment with the river.

of rich original geomorphological information and high ground resolution, but they are not accurate enough to be compared with the lidar data, and the width of a single view is limited, which makes geographic alignment complicated and can only be used to measure horizontal dislocations. However, KH-4B satellite data have the advantages of rich original geomorphological information and high ground resolution, but the accuracy is not enough compared with the LiDAR data. The width of single view in KH-4B satellite data is limited and the geographic alignment is complicated. It can only be used for horizontal dislocation measurement, and it is accompanied by noise when digitising. Therefore, this type of data has some limitations. Currently, modern datasets can be used in large quantities for areas in the western part of the country where the natural landscape has not been modified or has been modified only slightly. The previous application of KH-4B images shows that small dislocation volumes can be measured to obtain quantitative parameters of horizontal cumulative deformation (Jiang et al., 2017). For the modification areas, the joint use of KH-4B satellites and high-resolution datasets can be developed to jointly interpret active faults.

3.2. Data processing

For the Landsat 8 OLI data, due to the high vegetation coverage in the study area and the fact that most of the interpreted tectonic structures are fractures with obvious linear features, the Landsat 8 B7(R), B5(G), and B4(B) bands, which are more sensitive to information on vegetation, soil, and geological structures, were selected for false-colour compositing so that the tectonic factors were highlighted as much as possible. Then, band 8, with a resolution of 15 m, was subjected to 85° directional filtering to obtain a medium resolution remote sensing image with an outstanding linear structure. The image is close to natural colour, with moderate contrast and clarity, and this image can be used as the basic image for subsequent remote sensing interpretation. The remote sensing image is then mosaicked and cropped according to the distribution of fractures.

The KH-4B satellite data were obtained by digitizing black-and-white films, and the main processing workflow of image preprocessing was as follows: ① image cropping, ② image enhancement, ③ geographic alignment, and ④ image mosaicking. The fault traces of the XJF were

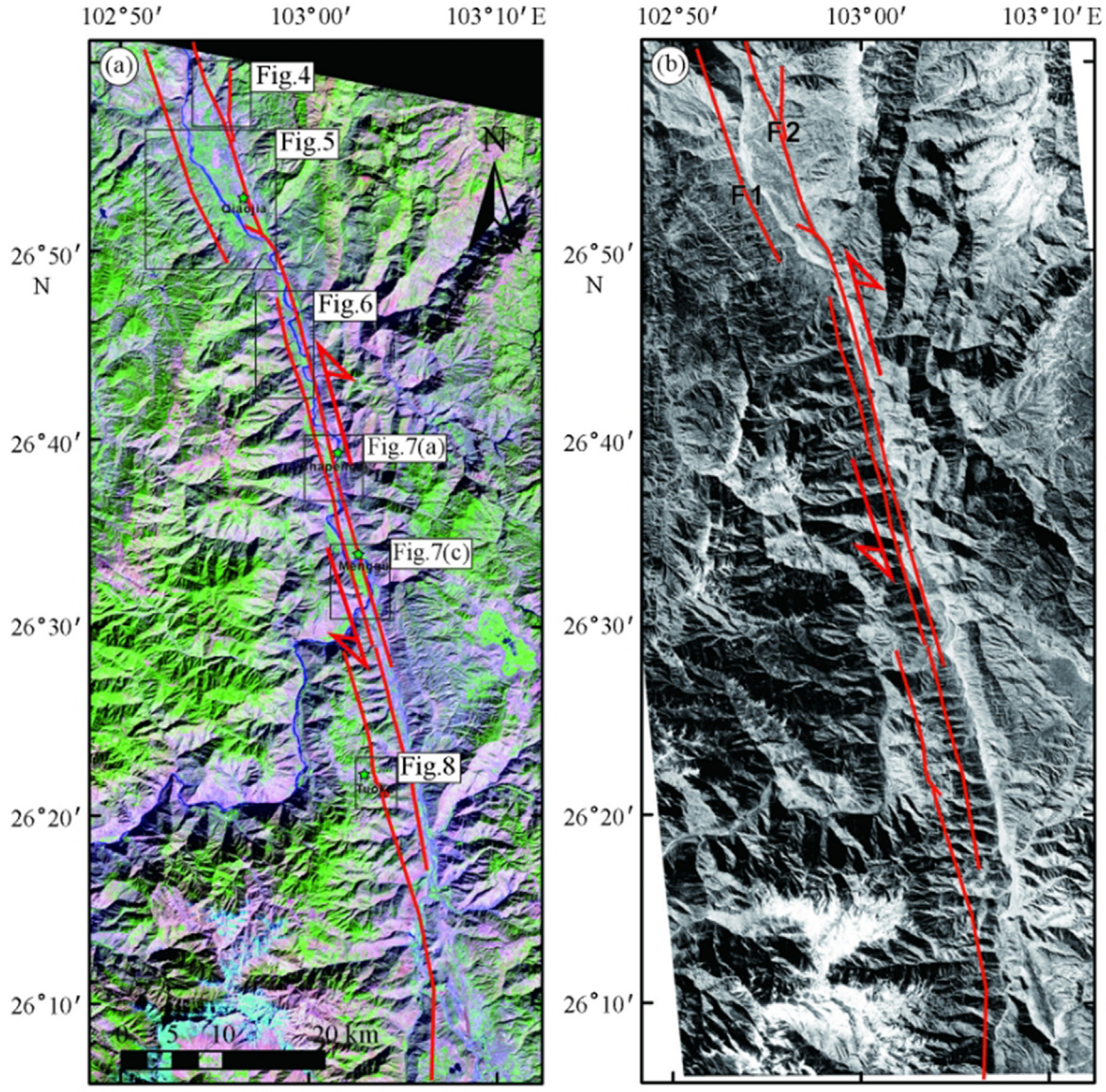

Fig. 3. Geometry of the Xiaojiang fault from interpretation of remote sensing images. (a) is a Landsat 8 image, and (b) is a KH-4B image. The black boxes represent locations of large-scale remote sensing interpretation.

first interpreted in detail based on surface features observed in the images, including fault scarps, surface fault ruptures, and offset linear landforms. When manually adding ground control points, we select control points to achieve geographic registration. However, due to the early imaging time of KH-4B, which was more than 50 years ago, the topography and geomorphology have changed greatly, and it is impossible to achieve accurate operation. Fault interpretation and measurement are affected by uncertainties, and control points are distributed as fully and evenly as possible. To reduce the influence of uncertainty, we select more points in areas with large changes in image edges or features.

4. Results and analysis of the interpretation

Based on the results of previous studies and remote sensing interpretation, the fault distribution map of the northern section of the Xiaojiang Fault Zone was obtained from imagery interpretation (Fig. 3a and b). In general, the northern section of the XJF can be divided into two parallel faults, approximately 4 km apart, with the eastern branch (F1), the Qiaojia fault (F2), located along the Jinshajiang Valley and the western branch located mainly within the mountain and extending southwards to the western branch of the middle section of the Xiaojiang fault (F1). Along the Jinsha and Xiaojiang Valleys, linear gullies have developed, and linear gullies can be observed in the fault that cuts through alluvial fan deposit, the water system in the left rotational feature or is deflected, and other phenomena. The Qiaojia fault (F2) controls the topographic transition zone of the foothills to form an intermountain basin or denudation surface in front of the high mountains, and the boundaries of the intermountain basin or denudation surface are mainly controlled by active faults, which are the main faults controlling the eastern side of the Jinsha Valley in terms of premountain topography. The West Branch Fault spreads throughout the mountain body, and the macro-geomorphology is not as significant as that of the Qiaojia fault (F2). However, the internal gullies on the mountain are characterized by significant left-hand rotation. Combined with previous geological survey results (Hu et al., 2023), the F2, which we interpreted has been verified in the field, and some of our interpretation results are consistent with those interpreted by predecessors using high-resolution Ladar data (Liu et al., 2016).

With respect to point one of the remote sensing interpretation, the whole image is near the north-south-oriented linear structure (Fig. 4). In the Landsat 8 (Fig. 4A) and KH-4B satellite images (Fig. 4B), fracturing is very obvious, the linear features are more prominent, and the tone and geomorphological contrast between the two sides of the fault are remarkable. In Landsat 8 images, the tone changes significantly (Fig. 4a), and the contrast is obvious. The left side of the fault in plan view has a purple tone, which shows relative subsidence. The right side has a green tone, which shows relative uplift (Fig. 4a). Along the fault, a series of gullies has developed and is accompanied by a left-rotating phenomenon, especially in the KH-4B image (Fig. 4b).

In terms of point two of the remote sensing interpretation, the fault strike is approximately N165°E, and the two faults are nearly parallel (Fig. 5). Both faults show left rotation along Jinsha Valley, forming the pull-apart basin (Fig. 5a). According to Landsat 8 satellite images, the area has been artificially modified, the original geomorphology has been destroyed, and the faint colour differences between the two sides of the faults is vague. The linear features are especially significant in the KH-4B satellite image, and the left-lateral geomorphology of some small rivers can be recognized. Fig. 5b shows the continuous leptokurtosis of the alluvial gullies, and the development of the steep canyon of the fault in Fig. 5C shows that the faults are vertically dislocated.

Remote sensing interpretation point three indicates that the faults are distributed mainly along the mountain front and that the overall strike has not changed, controlling the basin boundary (Fig. 6). This change is shown as a change in hue in the Landsat 8 image (Fig. 6a), and the linear feature of KH-4B is obvious (Fig. 6b). In the figure (Fig. 6c), we can see the continuous gully dislocation, the east side of the Xiaojiang River valley plain, with the development of a number of gully left dislocations, the west side of the mountainous areas of the development of some regions of fault scarp. The two large river flood fans show asymmetric shape, biased north side of the accumulation of significantly larger than the on south side.

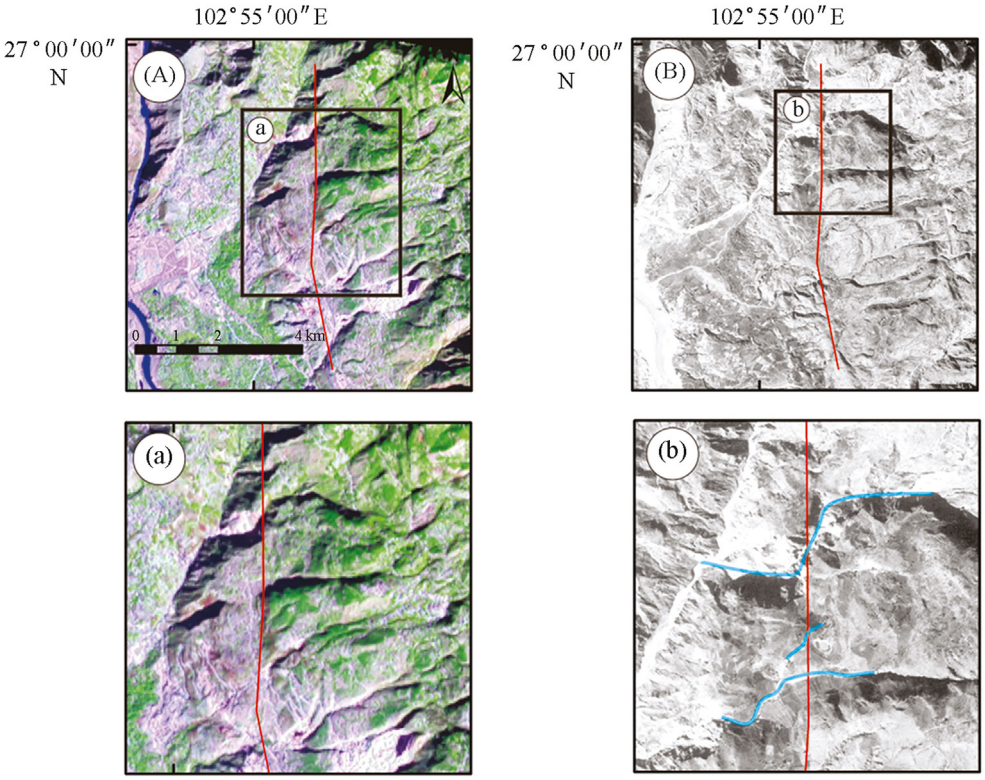

Fig. 4. Locations of points for large-scale remote sensing interpretation. (A) and (a) are the Landsat 8 satellite images; (B) and (b) are the KH-4B satellite images.

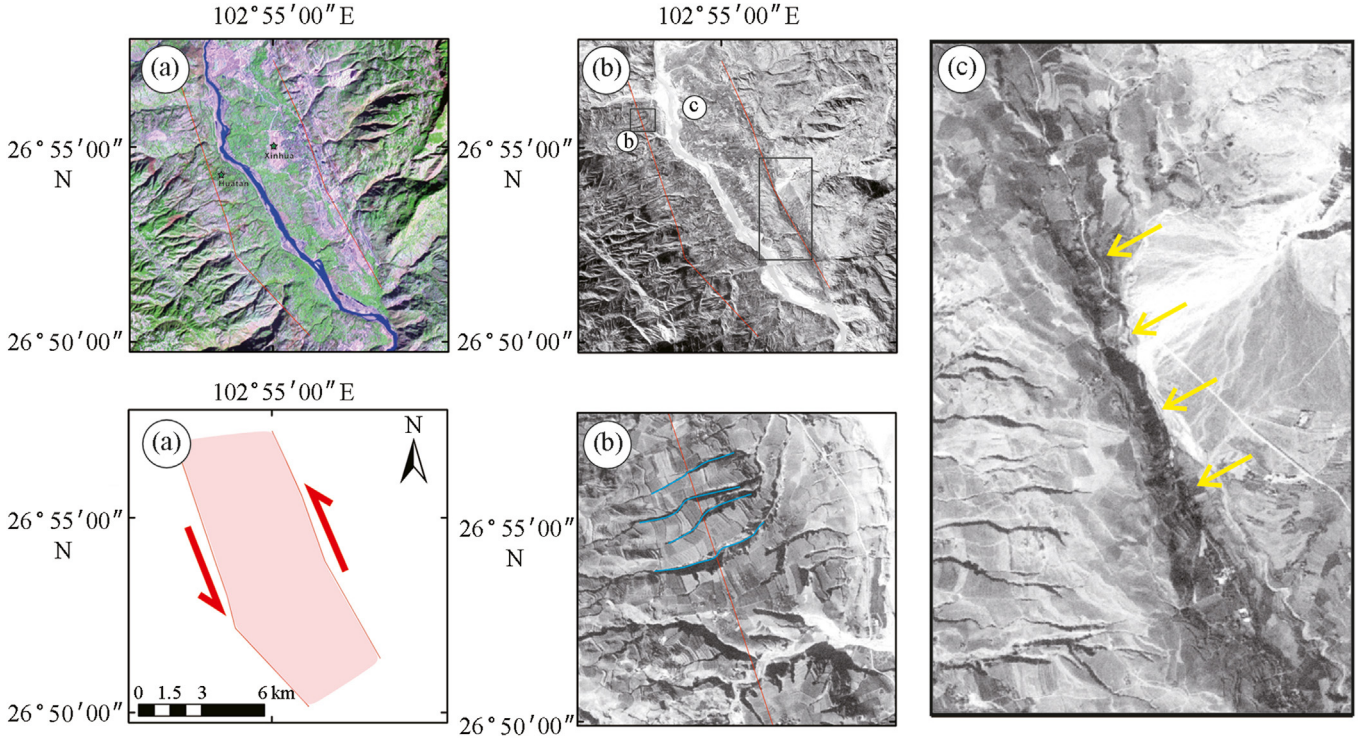

Fig. 5. Locations of points of large-scale remote sensing interpretation. (a) upper is the Landsat 8 satellite image; and (a) is the schematic diagram of the Lafen Basin; (b) and (C) are the KH-4B satellite images. In the figure, the red line represents faults and the blue line represents gullies.

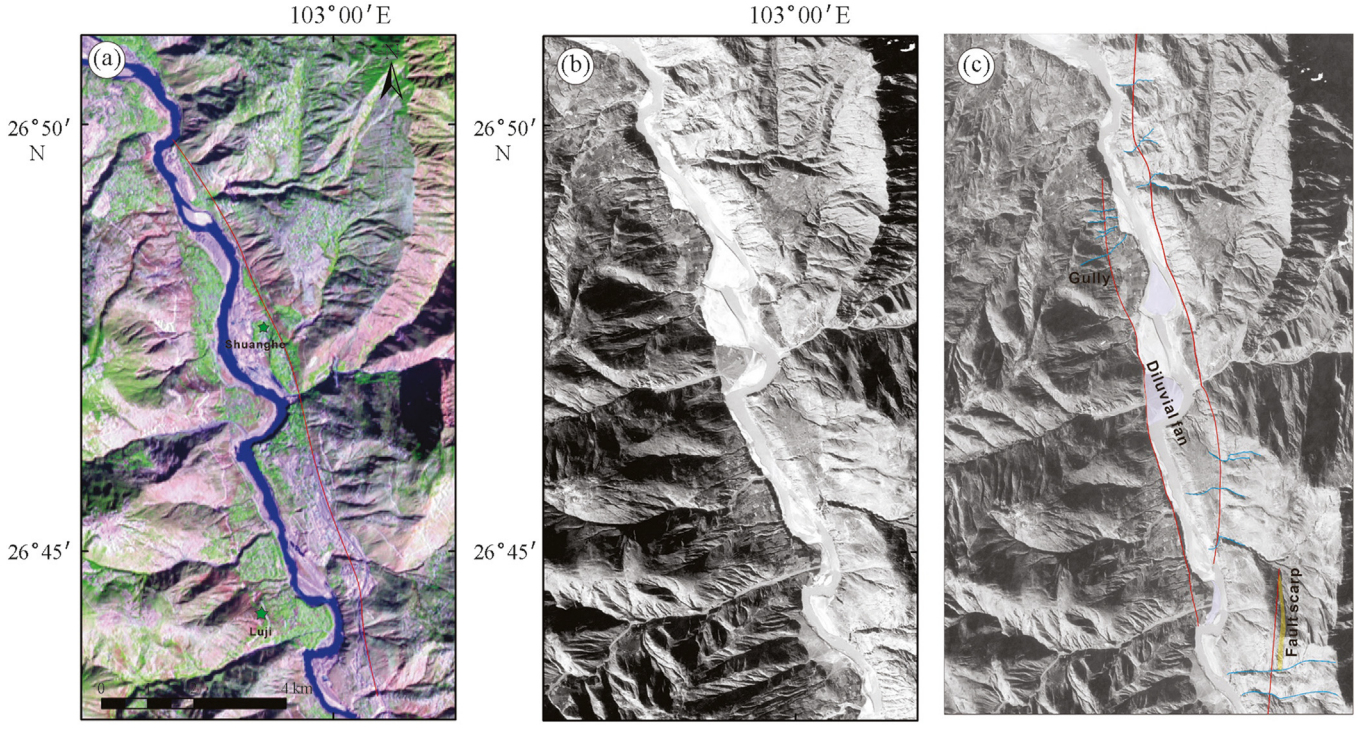

Fig. 6. Points of large-scale remote sensing interpretation. (a) is a Landsat 8 satellite image; (b) and (c) are the KH-4B satellite images, and the red lines represent faults.

Even in the distance from the flood fan, the north side of the Xiaojiang River has a similar fan accumulation, judged to be the original flood fan by the Xiaojiang rupture of the left dislocation to the place.

Remote sensing interpretation points four or five (Figs. 7 and 8). The Landsat 8 image clearly shows a change in hue (Fig. 7a and c), some segments of linear features are obvious (Fig. 7b and d), and the KH-4B

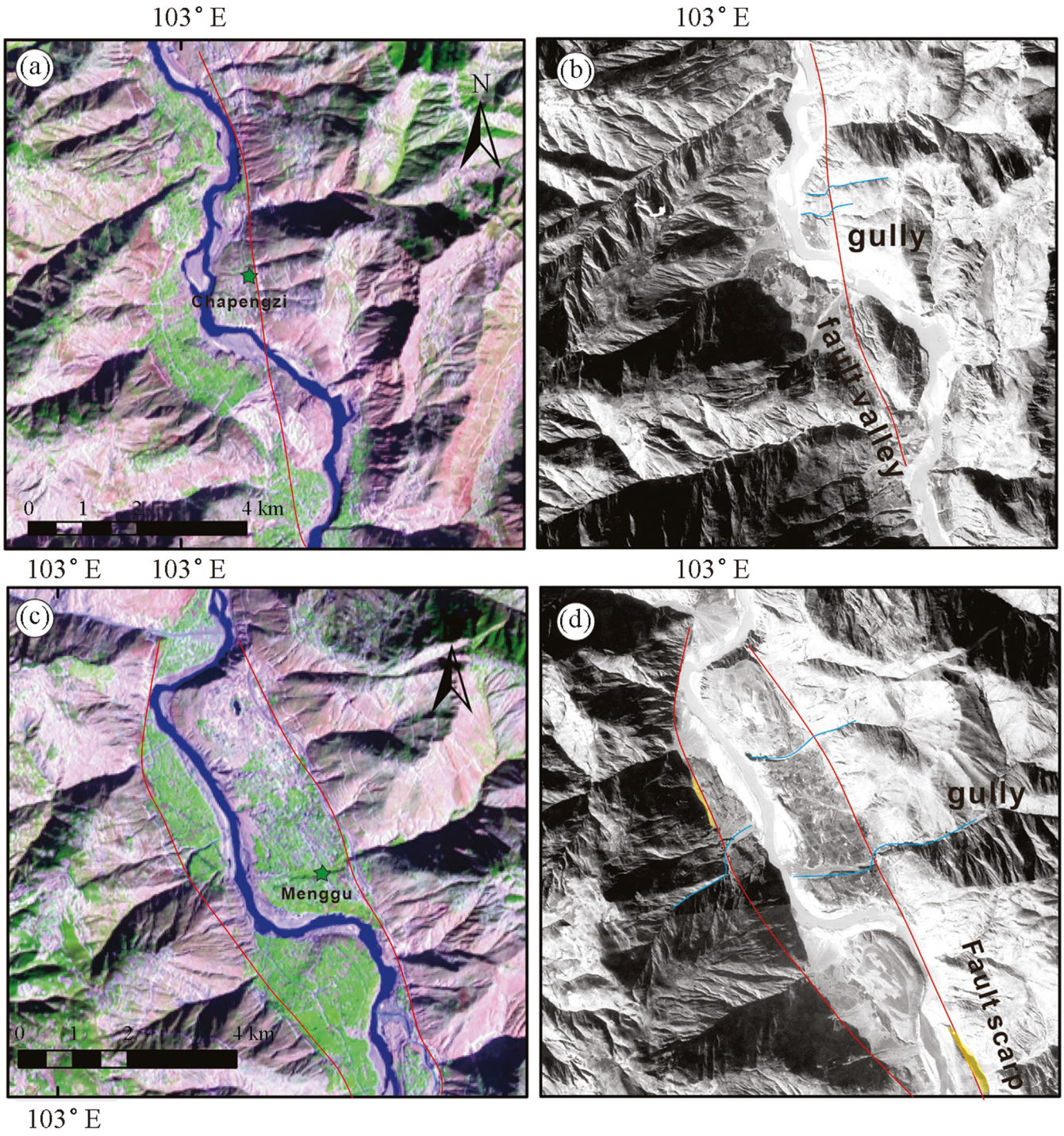

Fig. 7. Points of large-scale remote sensing interpretation. (a) and (c) are the Landsat 8 satellite images; (b) and (d) are the KH-4B satellite image. The red line represents the fault, and the blue line represents the gully.

image can be used to assess the geomorphological features better than the other images (Fig. 7b and 7d). The figure provides a clear view of gully left-lateral, faulted scarp, and fault valley landforms.

The fault at this point mainly spreads along the small basin in the mountain (Fig. 8), which is mainly manifested in the fault scarp, water system dislocation, and tilting of the basin surface (Fig. 8a). Tectonic uplift on the east side of the fault and descent on the west side form a small tectonic basin. Due to the local extrusion caused by the left-lateral dislocation, the river on the west plate of the fault exhibits twisting (Fig. 8b). In addition, the uplift of the eastern plate of the fault also forced the river to strongly downcut, resulting in the river on both sides of the steeper slope. The prominent landform in Fig. 8c is the fault escarpment, which is high in the east and low in the west, and the three gullies form a left-rotation dislocation at the fault scarp (Fig. 8d).

5. Discussion

5.1. Long-term average rate of slip of the northern section of the Xiaojiang fault

The geometric characteristics and slip rates of active faults are important for studying the kinematics and dynamics of faults and

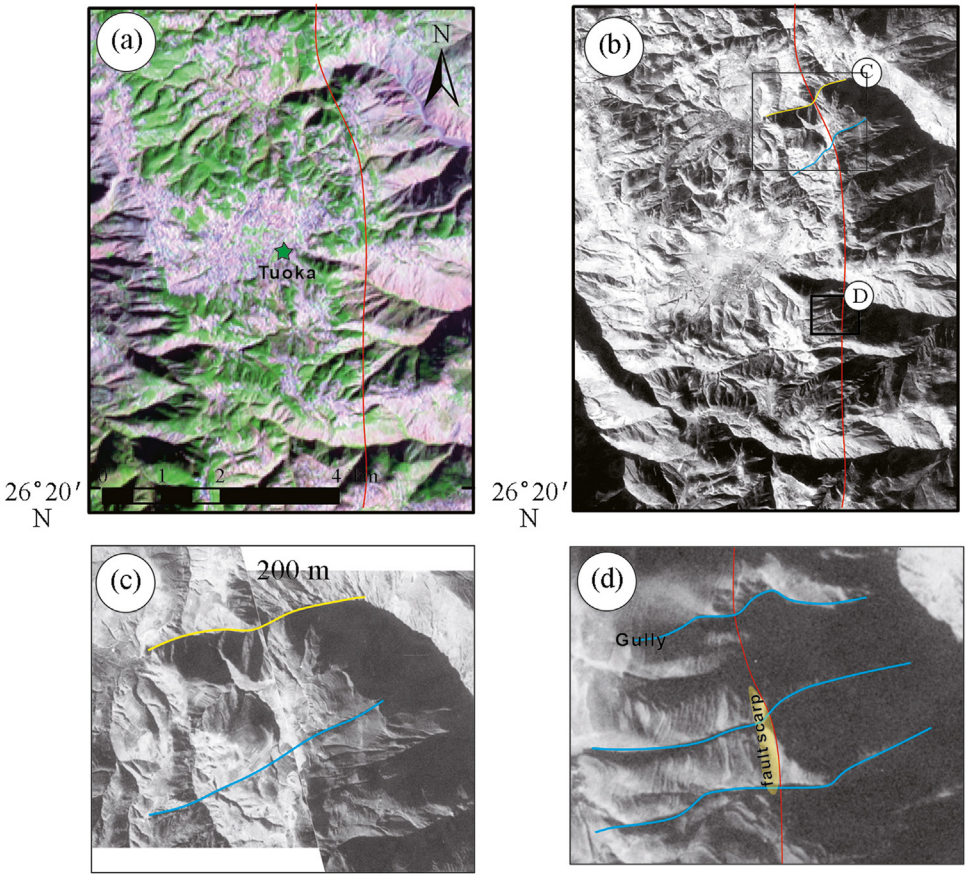

Fig. 8. Points of large-scale remote sensing interpretation. (a) is a Landsat 8 satellite image; (b), (c) and (d) are the KH-4B satellite images. The red line represents the fault, and the blue line represents the gully.

assessing their regional earthquake risk (Bai et al., 2022). The activity rates of active faults vary temporally and spatially (Friedrich et al., 2003; Chevalier et al., 2005). Accurately determining the activity rates of faults with different time scales and spatial distributions is important for understanding their kinematic characteristics and assessing their seismic hazard. The two main methods for determining the slip rate of fault zones are the traditional geological method and the geophysical method using data from GPS observation stations. The first method calculates the long-term average slip rate of the fault zone by assessing the displacements of different magnitudes accumulated over long-term tectonic movements and the time required to accumulate them. In contrast, the rate obtained by the second method reflects the slip rate of the fault zone in the present day period. The former characterizes the average slip rate over the long-term, while the latter represents the current slip rate of the zone. Only if the slip rate of the fault zone remains stable over an extended period will the GPS-observed rate be consistent with the long-term slip rate determined by geological methods.

Fault tectonics can cause staggered deformation of water systems and ridges across the fault zone during horizontal slip, and the accumulation of displacements due to fault slip and the superposition of multiple phases of activity over time have resulted in staggered torsional displacements of water systems and ridges at different scales, which are common in active fault zones (Zhao et al., 2019). Based on the torsion and dislocation of the ridge controlling the water system in the study area in the regional fault zone, the northern section of the XJF is characterized by obvious strike-slip movement, and the statistics of its detailed displacement are shown in Fig. 9.

The fault-zone displacements in the study area are concentrated within the range of 100 m–2 000 m. Previous researchers have studied rivers with displacements of 1 000 m–2 000 m, which generally developed fourth or fifth order terraces formed in the Middle Pleistocene over a period of about 150 000–200 000 years. Displacements of 500 m-1 000 m occurred since the Late Pleistocene, with the specific timing estimated to be about 100 000–80 000 years ago. Rivers or gullies with this magnitude of displacement developed second- and third-order terraces, and the estimated age of these terraces indicates they were formed in the Late Pleistocene. During the middle to late Late Pleistocene, left-lateral displacements of 200–500 m were observed, resulting in the development of second- and third-order terrace gullies. The onset of this development is dated to the middle-late Late Pleistocene, with 14C age results from previous researchers indicating that this type of gully developed 50 000–30 000 years ago (Song et al., 1998).

According to Song et al. (1998), the magnitude of displacement of the XJF in the study area can be categorized into three types: a displacement magnitude range of 1 000–2 000 m, which mainly represents the displacement of the XJF in the middle to late Pleistocene (200 000–150 000 years), and a displacement magnitude range of 500–1 000 m, which mainly represents the displacement magnitude since the middle to Late Middle Pleistocene (100 000–80 000 years), and a displacement magnitude range of 200–500 m, which mainly represents the displacement magnitude since the middle to late Pleistocene (50 000–30 000 years).

Based on the frequency statistics (Fig. 10), we suggest that 1 050 m is the amount of dislocation since the late Middle Pleistocene (200 000–150 000 years), 425 m is the amount of dislocation in the middle Late Pleistocene (100 000–80 000 years), and 300 m is the late Middle Late Pleistocene (50 000–30 000 years). Calculations using the displacements of the gullies and ridges and the time corresponding to their displacement magnitudes show that the long-term average slip rate of the northern section of the XJF in the study area has been 6.2 ± 1.1 mm/a

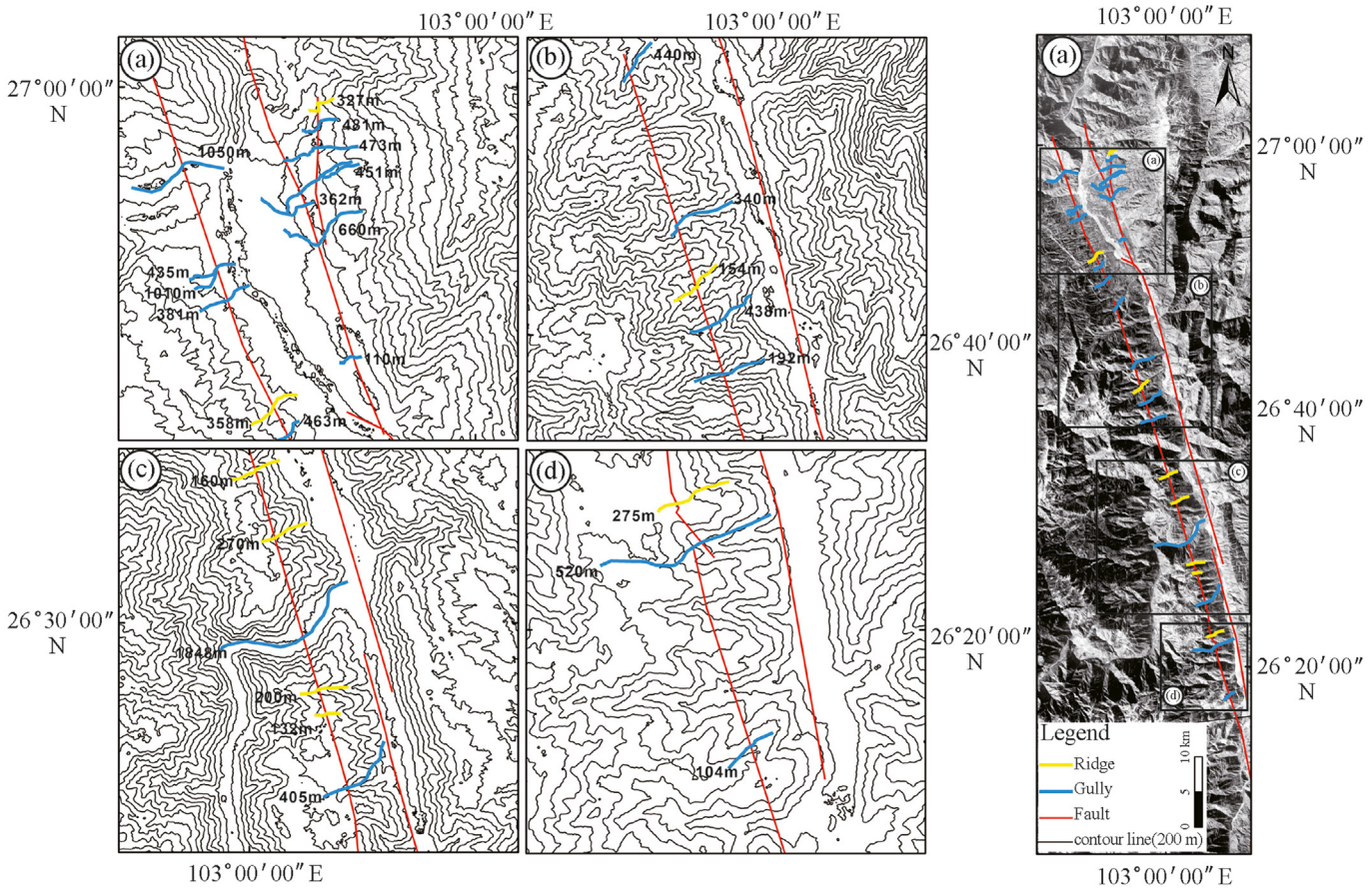

Fig. 9. Statistical map of ridge dislocations in Xiaojiang fault water system. The numbers in the figure represent dislocation scales.

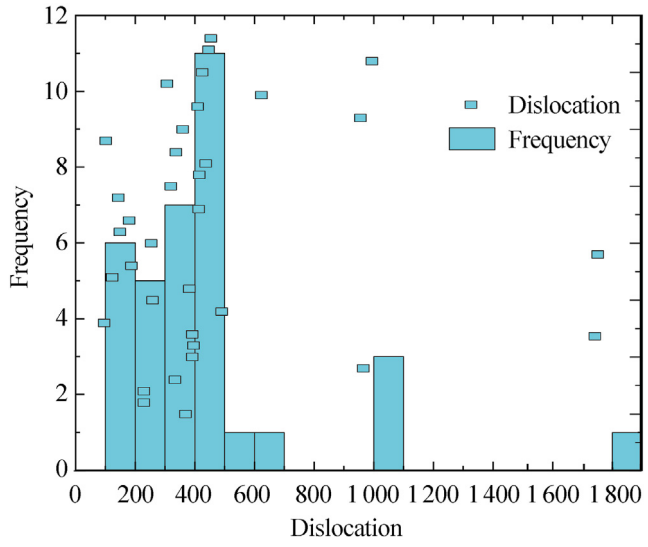

Fig. 10. Frequency graph of river ridge dislocation statistics.

since the late Middle Pleistocene, 11.4 ± 2.8 mm/a since the middle Late Pleistocene, and 8.0 ± 2.0 mm/a in the middle-late Late Pleistocene.

Wang et al. (1998) assumed that the initial left-lateral slip of the XJF occurred at approximately 4–2 Ma and thus estimated that the left-lateral slip rate of the northern section of the XJF was 15–30 mm/a, whereas Huang (Huang, 2010) suggested that the late Quaternary slip rates of the northern section of the XJF were approximately 4–8.6 mm/a. Hu et al. (2023) suggested that the slip rate of the northern section of the Xiaojiang Fault Zone is 13.2 ± 2.0 mm/a since 11.2 Ka, 11.5 ± 1.5 mm/a since 21.4 Ka in the Late Pleistocene, and that the overall slip rate during the Late Quaternary period is 10–13 mm/a, and Wen et al. (2011) obtained the slip rates of the northern section of the Xiaojiang Fault Zone from the inversion of the GPS data 10 mm/a, which represents the state of movement in the present day and does not represent the long-term geological rate.

As shown in Fig. 11, the slip rate of the XJF has gradually increased since the late Middle Pleistocene(150 Ka), with higher rates observed during the middle Late Pleistocene and the Holocene. By collecting quartz grain samples from the fault zone and conducting statistical analyses of erosion and micro-morphological features (Kanaori et al., 1985), it was confirmed that the fault's activity was primarily concentrated in the Late Pleistocene. Additionally, an analysis of sediments in the Qiaojia Basin supports the conclusion that the northern section of the XJF has entered a phase of intense tectonic activity since 120 Ka (Tai et al., 2024), which aligns with the slip rates obtained in this study.

5.2. Mechanism of the dynamics of the northern section of the Xiaojiang fault

The high slip rate of the XJF is closely related to dynamic processes of the Qingzang Plateau. In the collision between the Indian Plate and the Asian-European Plate, the Qingzang Plateau was strongly extruded and deformed, and the material inside the Qingzang Plateau was extruded eastwards, which was strongly blocked by the South China Block (Guo et al., 2024), resulting in southeastward movement of the Sichuan-Yunnan Block (Fig. 12A). The XJF is the eastern boundary of the Sichuan-Yunnan Block and is the main structure that accommodates the movement and deformation of the Sichuan-Yunnan Block. The rhombic Sichuan-Yunnan Block is further divided into subblocks in north-western

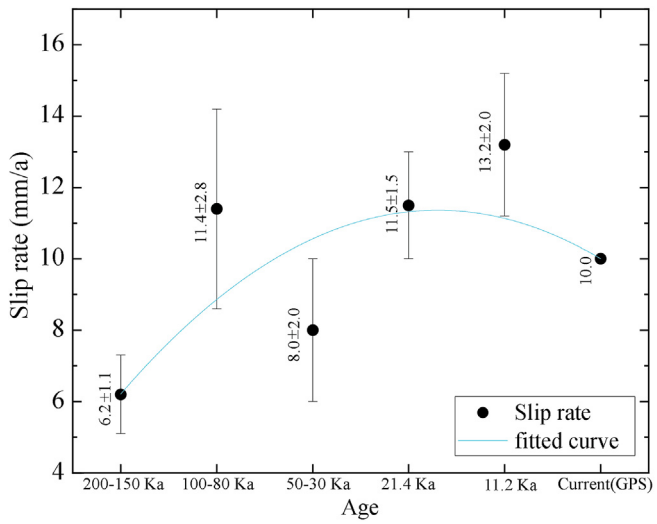

Fig. 11. Slip rate trend diagram.

Sichuan and central Yunnan by the Lijiang Xiaojinhe Fault. The eastern part of the central Yunnan subblock is bounded by the Anninghe fault, Zemuhe fault, and Xiaojiang fault, which feature left-rotating strike-slip faults, and the western boundary is bounded by the Red River fault, which features right-rotating strike-slip faults, with a strike-slip rate of approximately 3 mm/a. When the block is controlled by nearly parallel slip faults with opposite slip properties but unequal absolute values of slip rates, strong extrusion occurs on the boundary fault at the front end of the block's movement, with a slip component that is consistent with the slip properties of the boundary fault on the side where the absolute value of the slip rate is greater (Xu et al., 2003a, 2003b).

As the two subparallel boundaries in the central Yunnan subblock, the slip rate of the northern section of the XJF is significantly greater than that of the northern section of the Red River fault, which leads to clockwise rotation of the central Yunnan subblock in the process of translation in the southeast direction (Fig. 12). Under these conditions, the northern section of the XJF is involved in continuous extrusion, and a fault steeple formed during the extrusion process. According to the inversion of GPS data, the Xiaojiang Fault Zone is dominated by left-rotating strike-slip motion with a local component of extrusion (Zheng et al., 2017; Wang et al., 2008; Cheng et al., 2012). The northern section of the XJF was involved in extrusion from the middle Pleistocene to the Holocene, and once extrusion reached a certain level, this vertical motion almost stopped and was converted to horizontal motion. This resulted in the slip rate of the northern section of the XJF gradually increasing from the late middle Pleistocene to the Holocene.

Combined with the present-day GPS velocity field relative to the South China Block (Fig. 12B), the subblock in central Yunnan was blocked by the South China Block, which led to the subblock in central Yunnan moving only southwards, resulting in the present day slip rate of the XJF becoming larger. The most recent activity on the northern section of the XJF is characterized by left-rotating strike-slip faulting due to strong extrusion, representing the local strain response of the central Yunnan sub-block rotating clockwise along the boundary fault. This finding is consistent with the pattern of northwards and north-east wards thrusting of the Indian Plate leading to eastwards extrusion and the escape of material from the Qinghai-Xizang Plateau. To some extent, this reflects the coordination of tectonic deformation between block rotation and boundary fault slip in the Sichuan-Yunnan area in the context of continental block extrusion on the Qinghai-Xizang Plateau. The Zemuhe fault connects to the northern section of the Xiaojiang fault, where fault deformation since the late Quaternary has been dominated by left-lateral strike-slip motion, and the most recent large earthquake in this fault zone was the 1850 AD earthquake, with a magnitude greater than 7 (Yu et al., 2001) and a coseismic offset of up to approximately 4 m along the Dajiayangzi (Guo et al., 2021; Shi et al., 2018; Wang et al., 1998a, 1998b). Previously obtained rates for the Zemuhe fault are highly variable, ranging from 5 mm/a to 12 mm/a. Recently, Li et al. (2021) reported that the slip rate of the Zemuhe fault is 6.4 mm/a, which is similar to the inverted strike-slip rate of 5.3 ± 2.4 mm/a reported by Li et al. (2014). Furthermore, this value is in keeping with the slip rate of 6.4 ± 0.6 mm/a reported by Xu et al. (2003a, 2003b). There is also considerable controversy over the paleoseismic recurrence behavior of the Zemuhe fault, with proposed recurrence periods ranging from 300 to 3000 a (Ren et al., 2010; Tian et al., 2008). Overall, we believe that the

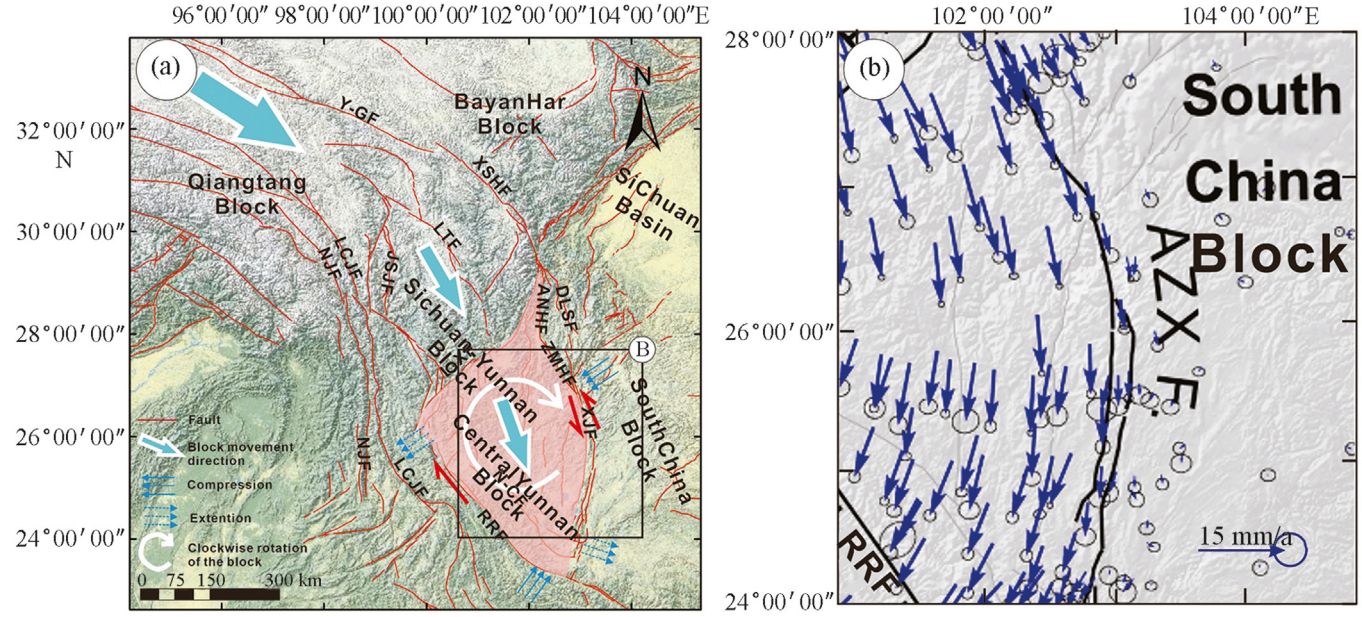

Fig. 12. Regional structural model. (a) Map showing Sichuan-Yunnan Block movement and the boundary rupture-slip pattern (modified from Guo et al., 2024 and Xu et al., 2003a); (b) Present-day GPS velocity field relative to the South China Block (modified from Li et al., 2021). AZXF: Anninghe-Zehuhe-Xiaojiang Fault Zone; RRF: Red River fault.

Zemuhe fault, with a left-lateral rate of 6.4 mm/a, has generated many large earthquakes. The Zhaotong-Ludian and Lianfeng Fault Zones are part of the boundary separating the SYB and the South China block and constitute the margin between the active and deformed secondary faulted block of Daliangshan and the relatively stable South China block (Wen et al., 2013). Recently, Wu et al. (2024) determined that the Lianfeng fault was active in the Holocene, and Li et al. (2021) proposed a slip rate of Zhaotong-Ludian fault is 2.4 mm/a. We suggest that the high slip rate of the northern section of the Xiaojiang fault is a combination of the slip rates inherited from the Zemuhe fault and the Zhaotong-Ludian fault.

The increased slip rate of the northern section of the Xiaojiang fault is closely related to neotectonic processes, driven by the counterclockwise rotation of the Sichuan-Yunnan block. This rotation is caused by the continuous lateral extensional extrusion along the southeastern margin of the Qinghai-Xizang Plateau.

6. Conclusion

This paper introduces the basic processing flow of KH-4B satellite data and uses remote sensing data to decipher the northern section of the Xiaojiang fault; identifies the markers for deciphering the fault by processing KH-4B satellite images and Landsat 8 images; utilizes a comparison of early remote sensing images and present-day Landsat 8 images; and combines the results with the previous results of the geometric distribution of the northern section of the Xiaojiang fault. This distribution was rearranged by comparing early remote sensing images with the present Landsat 8 images and combining them with previous research.

Moreover, the long-term average slip rate of the northern section of the Xiaojiang fault is 6.2 ± 1.1 mm/a since the late Middle Pleistocene, 11.4 ± 2.8 mm/a since the middle Late Pleistocene, and 8.0 ± 2.0 mm/a in the middle to late Late Pleistocene. The current slip rate of the north section of the Xiaojiang fault is relatively high, and there has not been a large earthquake in recent years. Thus, the seismic risk is high, which needs attention.

KH-4B imagery retains the original topography and geomorphology, which can reveal the geomorphology of faults that were not destroyed many years ago and play an important role in studying active faults, thereby providing new data for future studies of active tectonics.

CRediT authorship contribution statement

Xingao Li: Writing – review & editing, Writing – original draft, Visualization, Software, Resources, Project administration, Methodology, Investigation, Formal analysis, Data curation, Conceptualization. **Zhongtai He:** Writing – review & editing, Writing – original draft, Supervision, Resources, Project administration, Methodology, Investigation, Funding acquisition, Formal analysis, Data curation, Conceptualization. **Long Guo:** Writing – original draft, Visualization, Software, Resources. **Linlin Li:** Writing – original draft, Supervision, Software, Resources, Conceptualization.

Author agreement and acknowledgment

I would like to declare on behalf of my co-authors that the work described was original research that has not been published previously, and is not under consideration for publication elsewhere, in whole or in part. All the authors listed have approved the manuscript that is enclosed.

This work is supported by grants from the National Science and Technology Basic Resources Investigation Program of China [Grant Number 2021FY100104], the Seismogenic Structure Ex-ploration of Large Earthuqake [Grant Number DZ5WLD202301], the National Natural Science Foundation of China [Grant Number 41872227] and a research grant from the National Institute of Natural Hazards, Ministry of Emergency Management of China [Grant Number ZDJ2019-21].

Declaration of competing interest

The authors declare that they have no known competing financial interests or personal relationships that could have influenced the work reported in this paper.

References

Bai, M., Chevalier, M.-L., Li, H., Pan, J., Wu, Q., Wang, S., et al., 2022. Late Quaternary slip rate and earthquake hazard along the Qianning segment, Xianshuihe fault. Acta Geol. Sin. 96, 2312–2332. https://doi.org/10.19762/j.cnki.dizhixuebao.2022144.

Bi, H., Zheng, W., Zhang, P., Zeng, J., Shao, Y., Yao, Y., Lei, Q., Peng, H., 2022. Recovering surface slip distribution along the sertengshan piedmont fault (northern China) from airborne LiDAR data. Tectonics 41 (8). https://doi.org/10.1029/2021tc007174.

Burchfiel, B.C., Wang, E., 2003. Northwest-trending, middle Cenozoic, left-lateral faults in southern Yunnan, China, and their tectonic significance. J. Struct. Geol. 25, 781–792. https://doi.org/10.1016/s0191-8141(02)00065-2.

Chang, Y.Q., Chen, L.C., Li, X., et al., 2021. The Late Quaternary activity of the fault along the western margin of the Yiliang Basin of the Xiaojiang fault zone. J. Seismol. Res. 44, 152–161.

Cheng, J., Xu, X., Ren, J., Zhang, S., Wu, X., 2021. Probabilistic multi-segment rupture seismic hazard along the Xiaojiang fault zone, southeastern Tibetan Plateau. J. Asian Earth Sci. 221, 104940. https://doi.org/10.1016/j.jseaes.2021.104940.

Cheng, J., Xu, X.W., Gan, W.J., Ma, W.T., Chen, W.T., Zhang, Y., 2012. Block model and dynamic implication from the earthquake activities and crustal motion in the southeastern margin of Tibetan Plateau. Chin. J. Geophys. 55, 1198–1212.

Chevalier, M.L., Ryerson, F.J., Tapponnier, P., Finkel, R.C., Van Der Woerd, J., Li, H., et al., 2005. Slip-rate measurements on the Karakorum Fault may imply secular variations in fault motion. Science 307, 411–414. https://doi.org/10.1126/science.1105466.

Dong, P., 2015. LiDAR data for characterizing linear and planar geomorphic markers in tectonic geomorphology. J. Geophys. Rem. Sens. 4, 1–5.

Friedrich, A.M., Wernicke, B.P., Niemi, N.A., Bennett, R.A., Davis, J.L., 2003. Comparison of geodetic and geologic data from the Wasatch region, Utah, and implications for the spectral character of Earth deformation at periods of 10 to 10 million years. J. Geophys. Res. Solid Earth 108, 2199. https://doi.org/10.1029/2001jb000682.

Gold, R.D., Cowgill, E., Arrowsmith, J.R., Friedrich, A.M., 2017. Pulsed strain release on the Altyn Tagh fault, northwest China. Earth Planet Sci. Lett. 459, 291–300. https://doi.org/10.1016/j.epsl.2016.11.024.

Guo, L., He, Z., Ren, Z., Li, L., Li, X., Ji, H., et al., 2024. Recent Holocene activity and regional tectonic significance of the northern segment of the Red River fault zone. J. Struct. Geol. 185, 105194. https://doi.org/10.1016/j.jsg.2024.105194.

Guo, P., Han, Z., Dong, S., Mao, Z., Hu, N., Gao, F., Li, J., 2021. Latest quaternary active faulting and paleoearthquakes on the southern segment of the Xiaojiang Fault Zone, SE Tibetan plateau. Lithosphere 2021, 7866379. https://doi.org/10.2113/2021/7866379.

Han, Z.J., Dong, S.P., Mao, Z.B., et al., 2017. The Holocene activity and strike-slip rate of the southern segment of Xiaojiang Fault in the southeastern Yunnan region, China. Seismol. Geol. 39, 1–19.

Hu, M.M., Wu, Z., Li, J., Huang, X., et al., 2023. The late Quaternary strike-slip rate of the Qiaojia segment of the Xiaojiang fault zone. Acta Geol. Sin. 97 (1), 16–29.

Huang, F.G., 2010. Seismicity in Yunnan. Yunnan Science and Technology Press, Kunming.

Jiang, W., Zhang, J., Han, Z., Tian, T., Jiao, Q., Wang, X., et al., 2017. Characteristic slip of strong earthquakes along the Yishu fault zone in East China evidenced by offset landforms. Tectonics 36, 1947–1965. https://doi.org/10.1002/2016tc004363.

Jiang, W.-l., 2018. Holocene Rupture Pattern, Seismic Recurrence Feature of the Lenglongling Fault Zone and its Tectonic Implication for the Northeast Tibetan Plateau. Institute of Geology, China Earthquake Administration.

Kanaori, Y., Tanaka, K., Miyakoshi, K., 1985. Further studies on the use of quartz grains from fault gouges to establish the age of faulting. Eng. Geol. 21 (1–2), 175–194.

Kanaori, Y., 1985. Surface textures of intrafault quartz grains as an indicator of fault movement. Catena 12 (4), 271–279.

Li, K., Li, J., Ma, X., Li, X., 2020. The application of multi-source remote sensing image in the study of active faults – taking Xiaojiang Fault Zone as an example. Urban Geol. 15, 342–350.

Li, X., Xu, X., Ran, Y., Cui, J., Xie, Y., Xu, F., 2015. Compound fault rupture in the 2014 Ms 6.5 Ludian, China, earthquake and significance to disaster mitigation. Seismol Res. Lett. 86 (3), 764–774. https://doi.org/10.1785/0220140198.

Li, Y., Hao, M., Song, S., Zhu, L., Cui, D., Zhuang, W., Yang, F., Wang, Q., 2021. Interseismic fault slip deficit and coupling distributions on the Anninghe-Zemuhe-Daliangshan-Xiaojiang Fault Zone, Southeastern Tibetan Plateau, based on GPS measurements. J. Asian Earth Sci. 219, 104899. https://doi.org/10.1016/j.jseaes.2021.104899.

Li, Y.-H., Hao, M., Ji, L.-Y., Qin, S.-L., 2014. Fault slip rate and seismic moment deficit on major active faults in mid and South part of the Eastern margin of Tibet Plateau. Chin. J. Geophys. 57, 1062–1078. https://doi.org/10.6038/cjg2014040.

Liu, J., Ren, Z., Min, W., Ha, G., Lei, J., 2021. The advance in obtaining fault slip rate of strike-slip fault—a review. Earthq. Res. Adv. 1 (4), 100032. https://doi.org/10.1016/j.eqrea.2021.100032.

Liu, Y., Liang, H., Cheng, F., 2016. Application of high resolution airborne lidar in xiaojiang active tectonics and geological disaster study. J. Geomechanics 22 (3), 747–759.

Mao, Y., Liu, Z., Ye, J., Li, Z., 2016. Analysis on strong earthquake risk of Xiaojiang fault zone. J. Seismol. Res. 39, 213–217.
Meng, Z., Liu, J., Xie, Z., Lü, Y., 2021. Analysis of the correlation between the temporal-spatial distribution of b-value and seismic hazard: a review. Prog. Geophys. 36, 30–38. https://doi.org/10.6038/pg2021EE0025.
Molnar, P., Tapponnier, P., 1978. Active tectonics of tibet. J. Geophys. Res. Solid Earth (B11), 5361–5375.
Molnar, P., Tapponnier, P., 1975. Cenozoic tectonics of Asia: effects of a continental collision: features of recent continental tectonics in Asia can be interpreted as results of the India-Eurasia collision. Science 189, 419–426. https://doi.org/10.1126/science.189.4201.419.
Reid, H., 1910. On Mass-Movements in Tectonic Earthquakes. The California Earthquake of April 18, 1906. Report of the State Earthquake Investigation Commission, p. 192.
Ren, Z., Lin, A., Rao, G., 2010. Late pleistocene–holocene activity of the Zemuhe Fault on the southeastern margin of the Tibetan plateau. Tectonophysics 495, 324–336. https://doi.org/10.1016/j.tecto.2010.09.039.
Schoenbohm, L.M., Burchfiel, B.C., Chen, L., 2006. Propagation of surface uplift, lower crustal flow, and Cenozoic tectonics of the southeast margin of the Tibetan Plateau. Geology 34, 813. https://doi.org/10.1130/g22679.1.
Scholz, C.H., 2019. The Mechanics of Earthquakes and Faulting. Cambridge university press.
Shi, X., Wang, Y., Sieh, K., Weldon, R., Feng, L., Chan, C.H., Liu-Zeng, J., 2018. Fault slip and GPS velocities across the Shan Plateau define a curved Southwestward crustal motion around the Eastern Himalayan syntaxis. J. Geophys. Res. Solid Earth 123, 2502–2518. https://doi.org/10.1002/2017jb015206.
Sieh, K.E., Jahns, R.H., 1984. Holocene activity of the san andreas fault at wallace creek, California. Bull.geol.soc.amer 95 (8), 883–896.
Song, F.M., Wang, Y.P., Yu, W.X., et al., 1998. The Active Fault Zone of Xiaojiang. Earthquake Press, Beijing.
Tai, Z., Xiang, F., Cheng, W., Wang, Y., Huang, H., Song, L., et al., 2024. Sedimentary stages of Quaternary diluvium in Qiaojia Basin and its indication to the activity of the northern section of Xiaojiang fault zone. J. Chengdu Univ. Technol. (Sci. Technol. Ed.) 51 (3), 418–427.
Tan, X., Liang, K., Ma, B., 2023. A review of research progress on the late Quaternary activities of the Xiaojiang fault zone. Technol. Earthq. Disaster Prev. 18, 757–772. https://doi.org/10.11899/zzfy20230410.
Tian, Q., Ren, Z.K., Zhang, J.L., 2008. Study of paleoearthquakes by combined trench on Zemuhe Fault around daqingliangzi, Xichang, sichuan. Seismol. Geol. 30, 400–411.
Wang, E., Burchfiel, B.C., Royden, L.H., Chen, L., Chen, J., Li, W., Chen, Z., 1998a. Late Cenozoic Xianshuihe-Xiaojiang, Red River, and Dali Fault Systems of Southwestern Sichuan and Central Yunnan, China. Geological Society of America, Boulder, Colorado.
Wang, E., Burchfiel, B.C., 2000. Late Cenozoic to Holocene deformation in southwestern Sichuan and adjacent Yunnan, China, and its role in formation of the southeastern part of the Tibetan Plateau. Geol. Soc. Am. Bull. 112, 413–423. https://doi.org/10.1130/0016-7606(2000)112<413:lcthdi>2.0.co;2.
Wang, E., Burchfiel, C.B., Royden, H.L., Chen, L., Chen, J., Li, W., et al., 1998b. Late Cenozoic Xianshuihe-Xiaojiang, Red River, and Dali Fault Systems of Southwestern Sichuan and Central Yunnan. Geological Society of America, China.
Wang, M., Hu, S., Ma, H., Liang, B., Zhang, J., L, R., 2024a. 3d structural modelling of the anninghe-zemuhe-xiaojiang fault zone in the eastern boundary of sichuan-yunnan block using multi-data and implicit modeling methods. Seismol. Geol. 46 (1), 19–34, 2024.
Wang, M., Wei, Z., Long, F., Chen, H., Li, S., 2024b. Fault geometry and kinematics at the intersection of the Zemuhe, Daliangshan and Xiaojiang faults. Front. Earth Sci. 12, 1433148. https://doi.org/10.3389/feart.2024.1433148.
Wang, X., Zhang, J.F., Jiang, W.L., Wang, D.H., 2018. Application of Keyhole satellite data in active fault study: a case example of Jiangsu segment of Tan-Lu fault zone. J. Remote Sens. 22, 233–246.
Wang, Y., Wang, E., Shen, Z., Wang, M., Gan, W., Qiao, X., et al., 2008. GPS-constrained inversion of present-day slip rates along major faults of the Sichuan-Yunnan region, China. Sci. China Earth Sci. 51, 1267–1283. https://doi.org/10.1007/s11430-008-0106-4.
Weldon, R.J., Sieh, K.E., 1985. Holocene rate of slip and tentative recurrence interval for large earthquakes on the San Andreas fault, Cajon Pass, southern California. Geol. Soc. Am. Bull. 96 (6), 793–812.
Wen, X.Z., Du, F., Long, F., et al., 2011. Tectonic dynamics and correlation of major earthquake sequences of the Xiaojiang and Qujiang-Shiping fault systems, Yunnan, China. Sci. China Earth Sci. 54 (10), 1563–1575.
Wen, X.-Z., Du, F., Yi, G.-X., Long, F., Fan, J., Yang, P.-X., Xiong, R.-W., Liu, X.-X., Liu, Q., 2013. Earthquake potential of the Zhaotong and Lianfeng fault zones of the eastern sichuan-yunnan border region. Chin. J. Geophys. 56, 3361–3372.
Wu, L., He, Z., Xu, D., Li, L., Guo, L., Li, X., 2024. Study on the late quaternary activity of the Jinyang-Ningnan segment of the Lianfeng Fault Zone. J. Struct. Geol. 178, 105014. https://doi.org/10.1016/j.jsg.2023.105014.
Xu, X.W., Wen, X.Z., Zheng, R., Ma, W., Song, F., Yu, G., 2003a. Latest tectonic change pattern of the active block in Sichuan-Yunnan area and its power source. Sci. China Earth Sci. 33, 151–162.
Xu, X.W., Wen, X.Z., Zheng, R.Z.M., Wen, Tao, Song, F.M., Yu, G.H., 2003b. Recent tectonic patterns and dynamic sources of active blocks in Sichuan-Yunnan Region. Sci. China E D. 33, 12.
Yan, C.G., Cao, J.Q., Chen, Y.K., et al., 2020. Fine crustal structures of Zhangjiakou—Bohai tectonic zone in Tianjin area revealed by a deep seismic reflection profile. Chinese J. Geophys 63 (12), 4431–4439. https://doi.org/10.6038/cjg2020O0175 (in Chinese).
Yi, G.X., Wen, X.Z., Su, Y.J., 2008. Study on the potential strong-earthquake risk for the eastern boundary of the Sichuan-Yunnan active faulted-block, China. Chin. J. Geophys. 51, 1151–1158. https://doi.org/10.1002/cjg2.1311.
Yu, W., Song, F., Wen, X., Li, C., 2001. Investigation of the surface rupture zone of the 1850 Xichang earthquake. Earthq. Res. 23, 346–350.
Zhang, J., Jiang, W., Tian, T., Wang, X., 2016. High resolution remote sensing application research in active fault surveying. Acta Seismol. Sin. 38, 386–398. https://doi.org/10.11939/jass.2016.03.006.
Zhang, P.-z., Li, C.-y., Feng-ying, M., 2008. Strath terrace formation and strike-slip faulting. Seismol. Geol. 1.
Zhang, P.-Z., Shen, Z., Wang, M., Gan, W., Bürgmann, R., Molnar, P., et al., 2004. Continuous deformation of the Tibetan Plateau from global positioning system data. Geology 32, 809. https://doi.org/10.1130/g20554.1.
Zhao, W.D., Zheng, Y., Zhang, H.N., et al., 2019. Remote sensing interpretation and spatial distribution characteristics of the Anhui segment of Tanlu fault zone based on multi-source data. Remote Sens. Land Resour 31, 79–87.
Zhao, Y.S., 2003. Principles and Methods of Remote Sensing Application Analysis. Science Press, Beijing.
Zheng, G., Wang, H., Wright, T.J., Lou, Y., Zhang, R., Zhang, W., et al., 2017. Crustal deformation in the India-Eurasia collision zone from 25 years of GPS measurements: crustal deformation in Asia from GPS. J. Geophys. Res. Solid Earth 122 (11).
Zielke, O., Arrowsmith, J.R., Grant Ludwig, L., Akciz, S.O., 2012. High-resolution topography-derived offsets along the 1857 Fort Tejon earthquake rupture trace, San Andreas fault. Bull. Seismol. Soc. Am. 102 (3), 1135–1154. https://doi.org/10.1785/0120110230.